Geochemistry Geophysics Geosystems G3
AN ELECTRONIC JOURNAL OF THE EARTH SCIENCES
Published by AGU and the Geochemical Society

*Article*
Volume 6, Number 9
9 September 2005
Q09009, doi:10.1029/2005GC000950
ISSN: 1525-2027

# Deformation in the diffuse India-Capricorn-Somalia triple junction from a multibeam and magnetic survey of the northern Central Indian ridge, 3°S–10°S

**R. K. Drolia**
*National Geophysical Research Institute, Uppal Road, Hyderabad 500007, India (kumardrolia@yahoo.co.in)*

**C. DeMets**
*Department of Geology and Geophysics, University of Wisconsin-Madison, Madison, Wisconsin 53706, USA (chuck@geology.wisc.edu)*

[1] We use new multibeam and magnetic observations from 3°S–10°S along the Central Indian ridge to describe morphotectonic features and spreading fabrics within the study area and quantify deformation across the diffuse India-Capricorn-Somalia triple junction. A megamullion adjacent to the Vityaz transform fault is the first reported for the northern Central Indian ridge. The principal transform displacement zone (PTDZ) of the Vema transform fault consists of several closely spaced faults that can be traced for more than 150 km. Serpentinite or volcanic intrusions that are offset by the Vema PDTZ have inferred ages of 30,000–45,000 years, testifying to the youth of active features on the valley floor. Abyssal hill orientations throughout the study area have remained constant since at least 4 Ma, implying little or no change in the opening direction during this period. Abyssal hills from opposite sides of the ridge have the same orientations within our 1°–3° errors, implying that slip along reactivated fracture zones in the diffuse triple junction neither significantly rotates nor shears the intervening seafloor. Transform fault azimuths in the survey area agree with the NUVEL-1 Africa-Australia slip direction but are 5°–9° clockwise from the Africa-India direction. In contrast, seafloor spreading rates in the study area agree better with the NUVEL-1 Africa-India predictions. These seemingly conflicting observations are reconciled by a model in which seafloor within the diffuse triple junction rotates about the India-Capricorn pole at angular rotation rates that increase monotonically from zero to the full rotation rate across the deforming zone.

**Components:** 9003 words, 19 figures, 1 table.

**Keywords:** India-Capricorn; seafloor deformation; seafloor spreading.

**Index Terms:** 3035 Marine Geology and Geophysics: Midocean ridge processes; 3040 Marine Geology and Geophysics: Plate tectonics (8150, 8155, 8157, 8158).

**Received** 28 February 2005; **Revised** 10 June 2005; **Accepted** 1 July 2005; **Published** 9 September 2005.

Drolia, R. K., and C. DeMets (2005), Deformation in the diffuse India-Capricorn-Somalia triple junction from a multibeam and magnetic survey of the northern Central Indian ridge, 3°S–10°S, *Geochem. Geophys. Geosyst.*, *6*, Q09009, doi:10.1029/2005GC000950.

## 1. Introduction

[2] Due to the critical role of mid-ocean ridges in the geological, biological, and geochemical evolution of the ocean basins, detailed mapping of the mid-ocean ridges has been a high priority of the marine geophysical community for the past few decades. Although much progress has been made in mapping seafloor spreading centers in the Pacific and Atlantic basins, modern shipboard geophysical surveys in the northern Indian Ocean along the Carlsberg and northern Central Indian

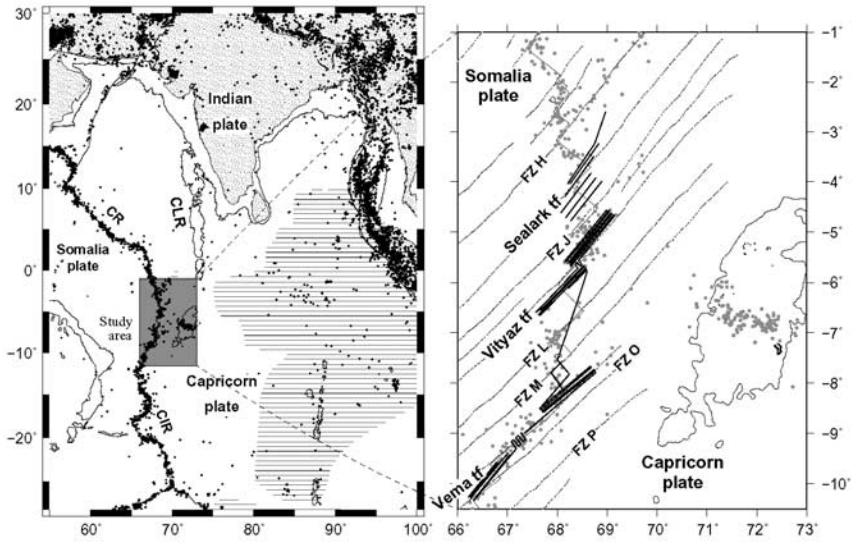


**Figure 1.** Location map and 1963–2004 earthquakes of all magnitudes above depths of 60 km. Patterned region south of India represents approximate limits of deformation associated with the wide India-Capricorn and Australia-Capricorn plate boundaries. Expanded view at right shows survey tracks for ORV *Sagar Kanya* 165 cruise and names of transform faults described in the text. Abbreviations: CR, Carlsberg Ridge; CLR, Chagos-Laccadive ridge; CIR, Central Indian ridge.

ridges have lagged well behind, partly due to their geographic isolation from most major oceanographic research centers. The unfortunate lack of observations from these two seafloor spreading centers has to date limited investigations into two important plate kinematic topics, the first being the spatial and temporal evolution of distributed seafloor deformation associated with the wide India-Capricorn oceanic plate boundary [*Wiens et al.*, 1985; *DeMets et al.*, 1994a, 2005] and the second being the recent history of India-Somalia seafloor spreading, which may contain useful information about the Himalayan orogen.

[3] Here, we use multibeam and magnetic data from a survey of the northern Central Indian ridge (Figure 1) to describe seafloor morphology in the survey area and study how the transition from India-Somalia motion to Capricorn-Somalia motion is accomplished across the diffuse Capricorn-Somalia-India triple junction. Collected in 2001 by the Indian research vessel ORV *Sagar Kanya*, the data consist of Hydrosweep swath bathymetry and total-field magnetic intensity profiles across six seafloor spreading segments and the Vema and Sealark transform faults (Figure 1). A key objective of this cruise was to map in detail the seafloor within the diffuse triple junction toward a better understanding of its kinematics over the past few Myr.

[4] An important goal of this paper is to employ the abyssal hill and transform fault orientations in the survey area to test between alternative models for deformation within the diffuse India-Capricorn-Somalia triple junction. In one model, the triple junction is discrete, implying that most or all India-Capricorn motion is accommodated by motion along a single structure or within a narrow zone east of the Central Indian ridge. Alternatively, motion may instead be distributed across a wide zone that defines a diffuse triple junction. Previous studies of earthquakes [*Bergman and Solomon*, 1984; *Wiens and Stein*, 1984; *Wiens*, 1986] and plate kinematic data [*Gordon et al.*, 1990; *DeMets et al.*, 1994a, 2005; *Royer et al.*, 1997] from this deforming region strongly favor the latter model, with a well-defined southern limit coinciding with the Vema fracture zone east of the ridge at 9°S and a more poorly defined northern limit possibly coinciding with Fracture Zone H at ~3°S. Kinematic models predict that India-Capricorn motion within the deforming crust west of the Chagos-Laccadive ridge consists predominantly of several millimeters per year of north-south extension, in accord with the uniformly oriented N-S tensional axes of earthquakes in this region [*DeMets et al.*, 1994a].

[5] Hereafter, we employ the plate name "Somalia" to refer to the plate directly west of the Central

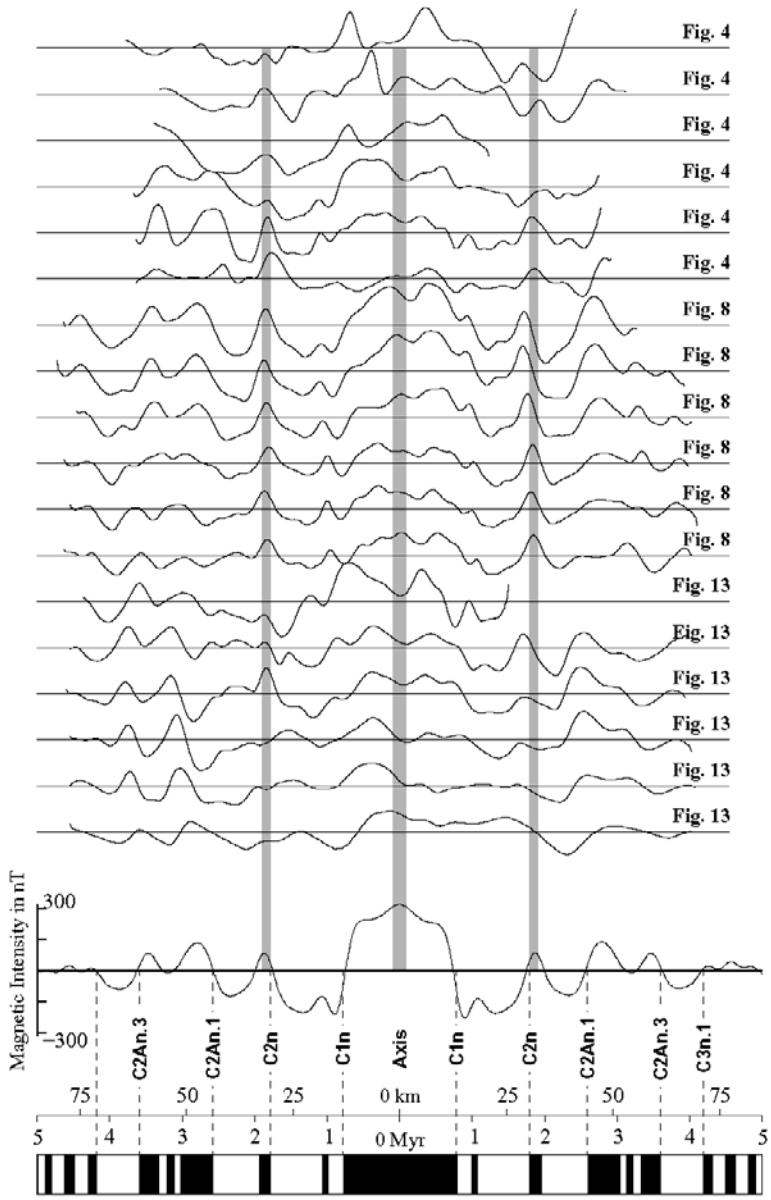


**Figure 2.** Summary interpretation of correlatable marine magnetic data from the *Sagar Kanya* 165 cruise. The same magnetic profiles are shown in map view in Figures 4, 8, and 13. Correlation tie points shown between the synthetic magnetic anomaly and magnetic block model at the bottom of the figure are shown in the interpretive diagrams of Figures 4, 8, and 13. Synthetic magnetic anomaly profile at bottom assumes 34 mm $yr^{-1}$ full spreading rate, 500-m-thick source layer, and 1-km-wide reversal transition zone.

Indian ridge (Figure 1), and the name "Capricorn" to refer to the plate east of the ridge and south of the Vema fracture zone. We also refer to these two plates as "Africa" and "Australia" in instances where we discuss the NUVEL-1A angular velocity vectors [*DeMets et al.*, 1994b]. The latter names reflect the common usage at the time that the NUVEL-1A model was published. For the purposes of this study, the plate names are interchangeable.

## 2. Hydrosweep and Magnetic Data

[6] The multibeam and magnetic observations presented below were collected during the ORV *Sagar*

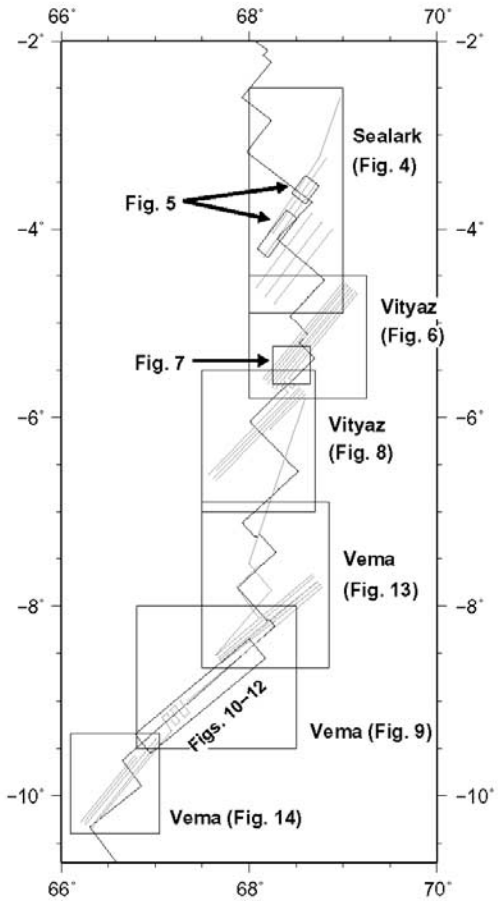


**Figure 3.** Guide to map locations for subsequent figures.

*Kanya* cruise 165 from May to July of 2001 as part of a targeted geophysical survey of the diffuse India-Somalia-Capricorn triple junction. The survey track lines provide good multibeam coverage of parts of six seafloor spreading segments and two transform faults (Figure 1), and extend out to average crustal ages of ~4 Ma (Figure 2). Transit tracks across two additional spreading segments and four transform faults were also made. We refer the reader to *Drolia et al.* [2003] for information about the data acquisition and preliminary data interpretation. For this study, we reprocessed the raw Hydrosweep travel times using MBsystem software [*Caress and Chayes*, 1996]. The 59-beam Hydrosweep sonar array illuminates a cross-track horizontal swath equal to approximately twice the water depth. For the water depths typical of our survey area (2000–6000 m), each of the 59 sonar beams images a cross-track swath that is 70 m to 200 m wide. The cross-track horizontal resolution of our data thus averages ~140 m. Relative depths are known to ~10–25 m, depending on how effectively the variations in water sound velocities are removed [*Caress and Chayes*, 1996].

[7] Following processing of the raw data, we employed large-scale maps, perspective views, and overlays of residual magnetic anomalies to interpret the multibeam data. From the large-scale maps, we digitized bathymetric lineations, focusing primarily on the surface traces of normal faults at the edges of abyssal hills and lineations within transform and fracture zone valleys. Abyssal hill lineation ages were estimated using opening-angle-versus-age flow lines constructed for each spreading segment. Seafloor spreading rates and ages were estimated from magnetic anomaly profiles reduced from total-field ship-board and aeromagnetic data from the survey region. Figure 2 summarizes the correlatable magnetic profiles from the *Sagar Kanya* 165 cruise. We supplemented these data with magnetic data from earlier *Sagar Kanya* cruises [*Drolia et al.*, 2000] and archived data described by *DeMets et al.* [2005]. All magnetic anomalies were reduced to the pole [*Schouten and McCamy*, 1972] to facilitate their interpretation.

## 3. Morphotectonics

[8] We first describe noteworthy aspects of the seafloor morphology in the survey area, proceeding systematically from the northern to the southern limits of the survey area. For organizational clarity, we divide the survey area into three general areas, corresponding to seafloor near the Sealark, Vityaz, and Vema transform faults (Figure 3). The northern Central Indian ridge in the study area consists of seven seafloor spreading segments, all offset by sinistral-slip transform faults whose lengths range from 50–240 km (Figure 1). Full spreading rates over the past few Ma have averaged a nearly constant 32–35 mm $yr^{-1}$ in the study region [*DeMets et al.*, 2005], comparable to opening rates along the southern Mid-Atlantic ridge. The general morphotectonic characteristics of seafloor and transform faults along the northern Central Indian ridge closely resemble those of other slow spreading centers. We thus focus principally on features that are either unique to the region or important for the ensuing kinematic analysis. The reader is also referred to *Kamesh Raju et al.* [1997] and *Drolia et al.* [2000, 2003] for earlier descriptions of the morphotectonics in this region.

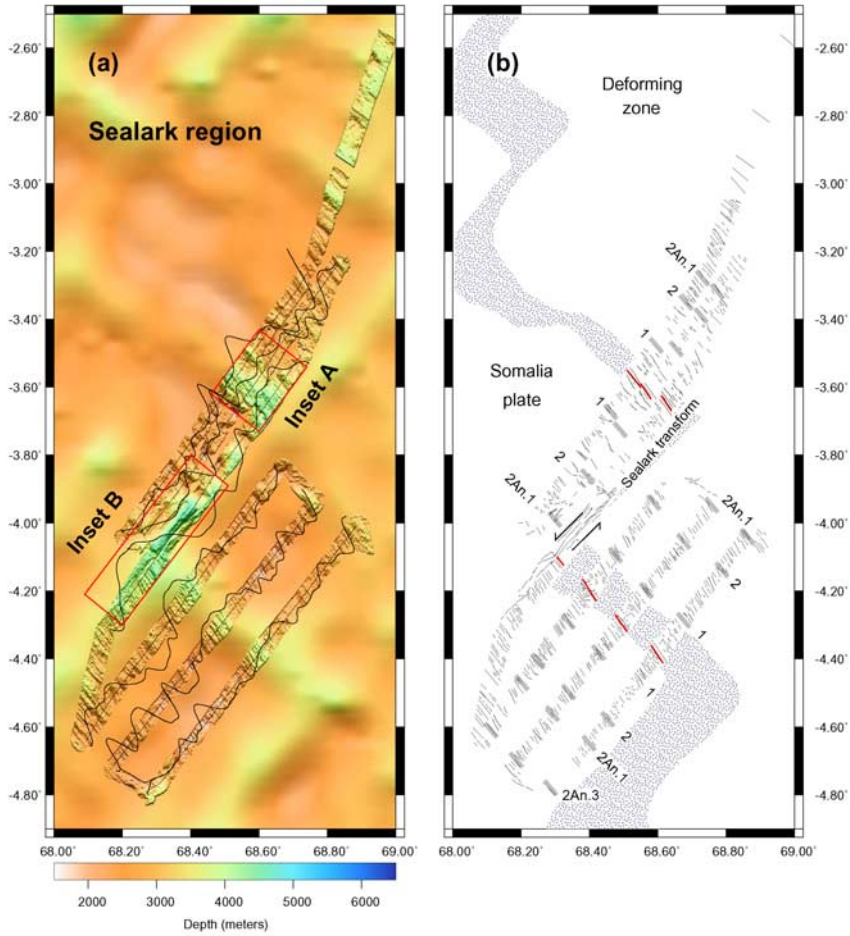


**Figure 4.** (a) Seafloor bathymetry and magnetic anomalies for the Sealark transform fault and flanking spreading segments. Detailed Hydrosweep bathymetry overlays 2-minute seafloor bathymetry [*Sandwell and Smith*, 1997]. Red boxes designate locations of insets A and B in Figure 5. Magnetic anomaly interpretations are shown in Figure 2. Positive magnetic anomalies point to the northwest. (b) Lineations interpreted from multibeam data. The neovolcanic zone, shown with red lines, is interpreted from the axial magnetic high and axial valley morphology. Wide shaded lines show correlations of anomaly 1 (0.78 Ma), the center of anomaly 2 (1.86 Ma), the young edge of anomaly 2An.1 (2.58 Ma), and the old edge of anomaly 2An.3 (3.60 Ma).

### 3.1. Sealark Transform and Nearby Spreading Segments

[9] Figure 4 shows Hydrosweep coverage of the Sealark transform fault and the spreading segments that terminate the fault. Only the southwestmost 25 km of the active portion of the 60-km-offset Sealark transform fault was insonified, revealing a 10 km-wide valley with average depths of 4600 m and a narrow, 150- to 200-m-high median ridge adjacent and parallel to the southeast edge of the valley (see inset B of Figure 5). Similar median ridges from the Kane transform valley in the northern Atlantic basin are interpreted by *Pockalny et al.* [1988] as fault-bounded blocks uplifted by serpentinization of mantle beneath the thin transform valley floor, possibly in response to localized compression within the transform tectonized zone or a change in the plate slip direction that placed the transform fault under compression. The data available to us do not permit a unique explanation for the origin of the median ridge in the Sealark transform valley.

[10] Although the principal transform displacement zone (PTDZ), where present-day strike-slip motion is accommodated [*Tchalenko*, 1970], is not clearly defined by our multibeam data, it may consist of several weakly defined and apparently discontinuous lineations that follow and may cut through the

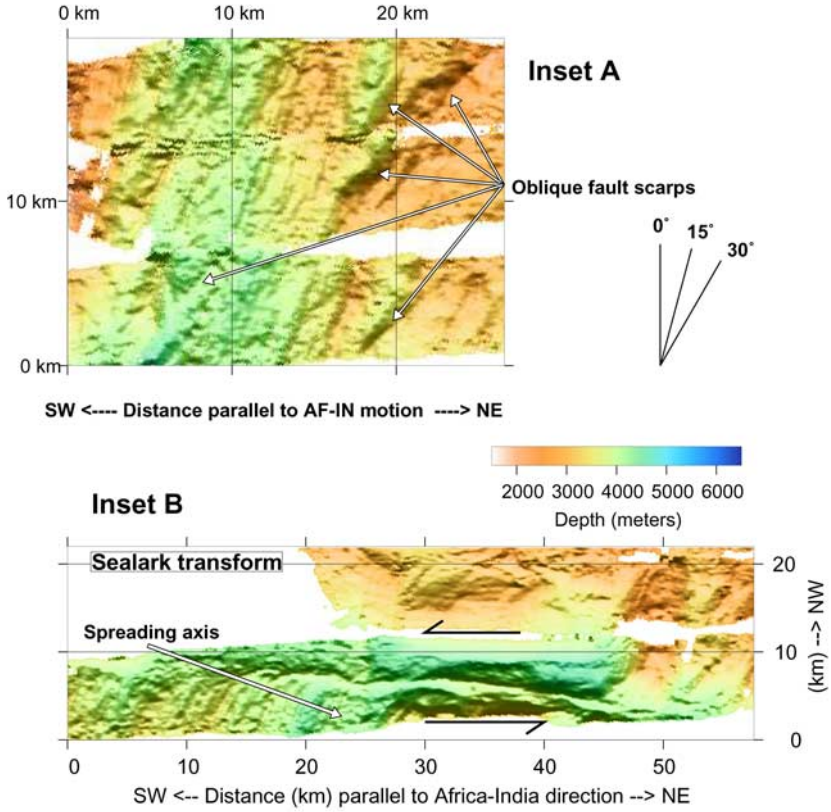


**Figure 5.** Oblique Mercator views of insets A and B from Figure 4. Both insets are projected around the NUVEL-1A Africa-India pole. Horizontal lines in the insets thus parallel the Africa-India slip direction, and vertical lines are lines of longitude emanating from the Africa-India rotation pole.

median ridge (from X = 34–40 km and X = 47–50 km in inset B of Figure 5). If the PTDZ coincides with the median ridge, the highly elongated median ridge is likely a product of strike-slip tectonism, possibly consisting of volcanics being extruded at the ridge-transform intersection (RTI) and entrained in the PTDZ. It seems unlikely that the PTDZ is located in the deep basin northwest of the median ridge (Figure 5) since there is no apparent path to continue sinistral slip northeastward out of the basin past the high-standing abyssal hill (at x = 47–50 km) that terminates the basin at its northeast end.

[11] The spreading segments that intersect the Sealark transform fault at its northeast and southwest ends (Figures 4 and 5) consist of several-kilometer-long en echelon axial volcanic ridges that are oriented ~10° CW from the general ~N45°W trend of the axial valley. Perspective views of the axial valleys at both ends of the Sealark transform fault (not shown) reveal several-hundred-meter-high volcanoes that coincide with the axial magnetic high, marking the present spreading axis. Prominent inward-dipping fault scarps located adjacent to and within the axial valley at the northeastern end of the Sealark (inset A, Figure 5) are rotated ~15–30° with respect to the overall trend of the spreading segment. The Hydrosweep coverage in this area is too limited to resolve the origin of these oblique features.

[12] The axial valleys of the spreading segments at both ends of the Sealark transform become progressively narrower and shallower with increasing distance from the RTIs, as noted by *Drolia et al.* [2003]. Similar variations in axial valley morphology are observed in the Atlantic basin, where seafloor spreading rates are comparable to those in our study area [*White et al.*, 1984; *Kuo and Forsyth*, 1988; *Lin et al.*, 1990; *Sempere et al.*, 1993]. Gravity and seismic refraction surveys of spreading segments from the southern Mid-Atlantic ridge strongly suggest that magma upwelling is focused beneath some segment centers [*White et al.*, 1984; *Kuo and Forsyth*, 1988; *Lin*

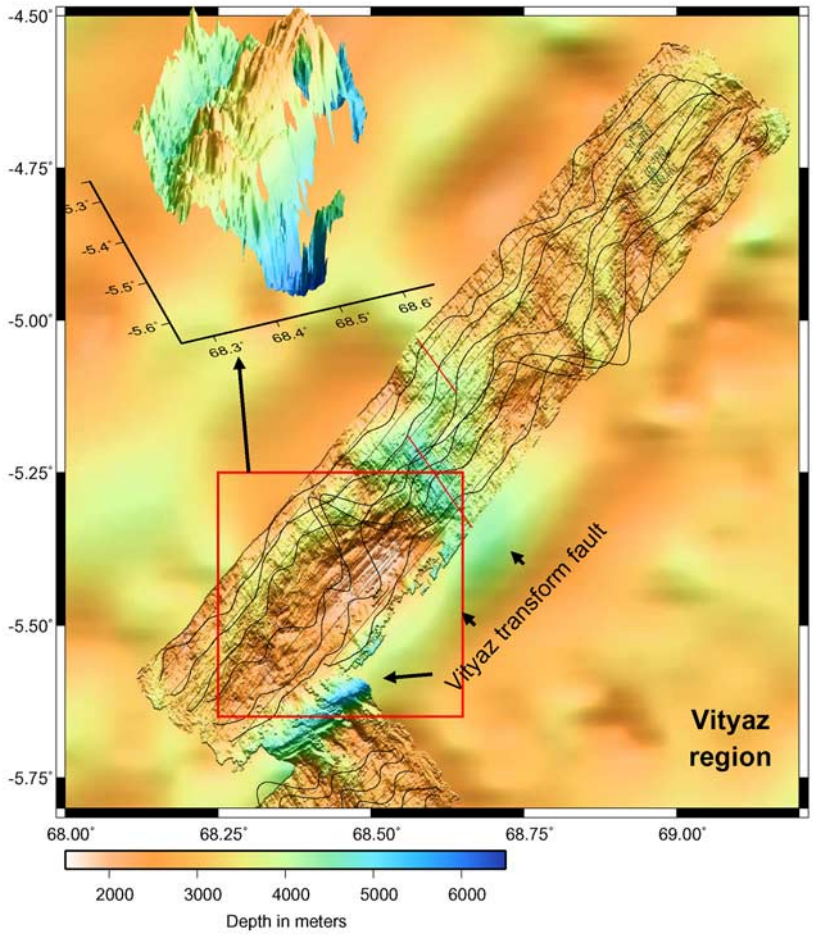


**Figure 6.** Hydrosweep seafloor bathymetry and magnetic anomalies for spreading segment at northeast end of the Vityaz transform fault with perspective view of the Vityaz megamullion. Positive magnetic anomalies point to the northwest. Magnetic anomalies are not correlatable and hence are not shown in Figure 2.

*et al.*, 1990]. On the basis of these observations, *Shaw and Lin* [1996] use 3-D modeling of an idealized slow spreading segment for which magma upwelling is focused beneath the segment center to demonstrate that the observed widening and deepening of the axial valley near the RTIs is a likely consequence of progressive thinning of the crust toward the RTIs. We thus conclude that the along-axis variations in axial valley morphology that we observe are caused by magma-dominated versus magma-starved extension.

## 3.2. Spreading Segments and a Megamullion Near the Vityaz Transform

[13] Closely spaced track lines that cross the spreading segments at the ends of the Vityaz transform fault afford an excellent view of an active megamullion at the inner northeastern corner of the Vityaz transform fault (Figure 6). The first described for the northern Central Indian ridge, the Vityaz megamullion is an inner corner, elongated domal high with well-expressed ridge-perpendicular corrugations. The megamullion rises from the 4700-m-deep rift axis to a depth of 2300 m over a distance of only 9 km (Figure 7), yielding a best slope estimate of 20° for this inward-facing slope. At distances beyond 13 km from the ridge axis, the slope reverses and the surface of the megamullion tilts gently (1.5°) away from the spreading axis. The well-defined linear corrugations on the surface of the megamullion have heights of a few tens of meters to 120 m (Figure 7). The morphologic characteristics of this megamullion fall within the ranges reported for Atlantic basin megamullions [*Tucholke et al.*,

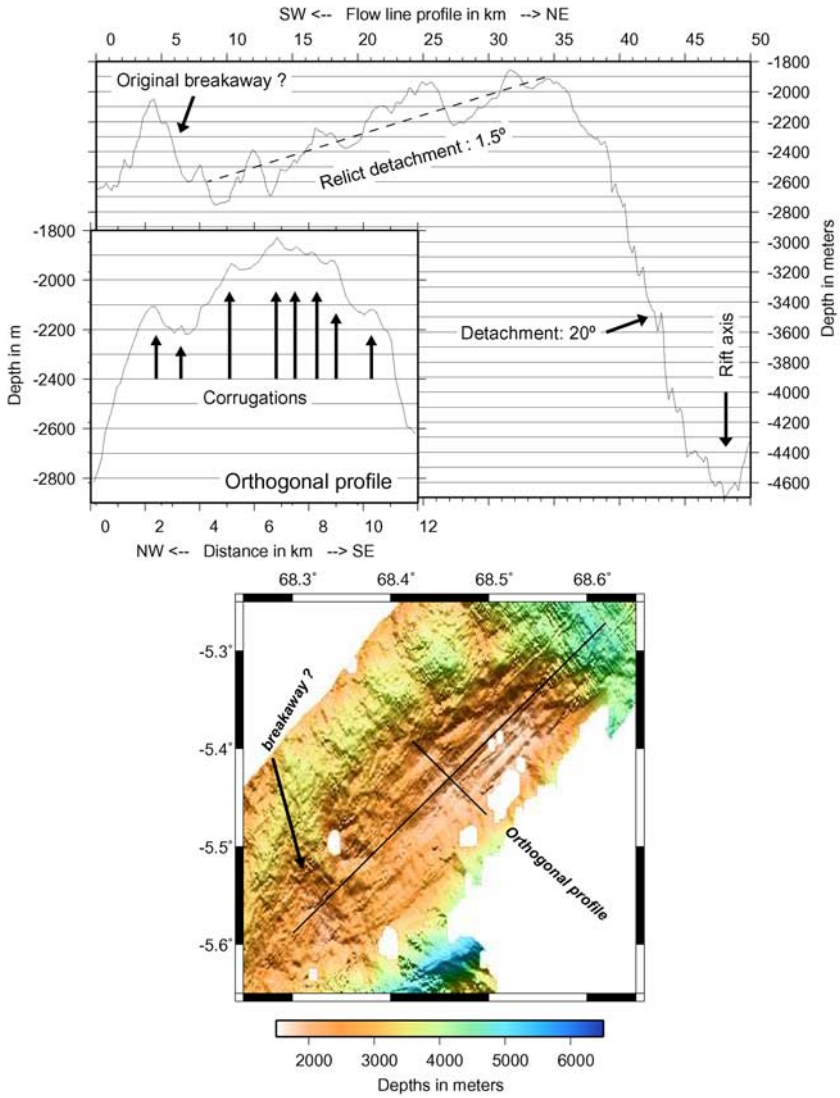


**Figure 7.** Map view of the Vityaz megamullion and depth cross sections based on profiles (black lines) shown in map view.

1998], which formed at comparably slow seafloor spreading rates.

[14] We interpret the Vityaz megamullion as an active (inner rift wall) detachment surface that accommodates extension across an amagmatic spreading segment, similar to published interpretations of other megamullions [i.e., *Dick et al.*, 1981; *Tucholke et al.*, 1998; *Ranero and Reston*, 1999]. The domal shape and reversal in the sense of dip of the detachment surface may result from progressive rotation of the footwall via isostatic uplift during its transport away from the ridge axis [*Tucholke et al.*, 1998]. Our data also do not permit us to exclude the possibility that normal faulting occurs along the side of the megamullion facing the adjacent Vityaz transform valley, where a nearly 4 km depth change occurs over a distance of only 15 km.

[15] We postulate that the fault breakaway, where extension initiated along the megamullion detachment surface, corresponds to a 700-m-high, inward facing scarp located ~45 km from the present spreading axis (Figure 7). For a half-opening rate of 17 km/Myr, the implied inception age for faulting along this presumed breakaway surface is ~2.6 Ma. A more precise age cannot be estimated because

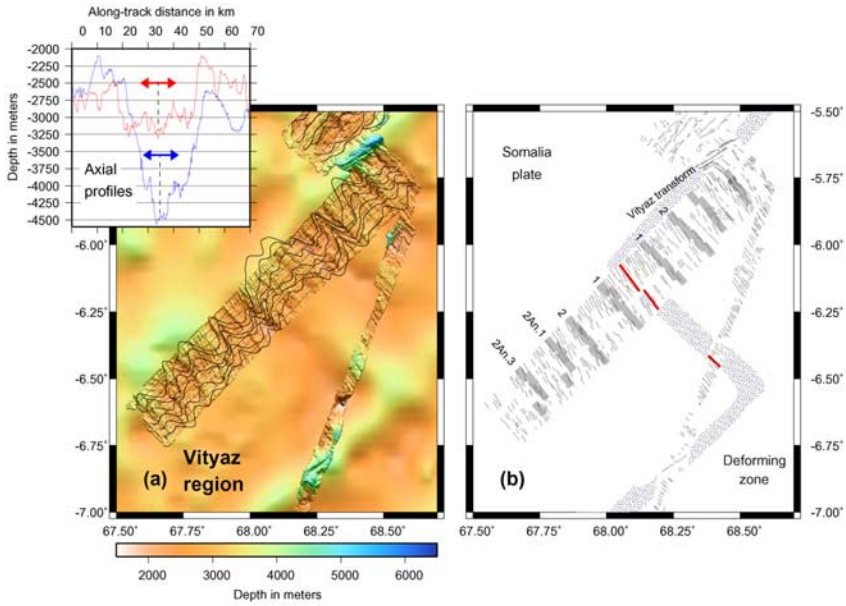


**Figure 8.** (a) Hydrosweep seafloor bathymetry and magnetic anomalies for spreading segment at southwest end of the Vityaz transform fault. Positive magnetic anomalies point to the northwest. Inset shows ridge-normal depth profiles across the spreading segments at the northeastern (blue line) and southwestern (red line) ends of the Vityaz transform fault. Vertical dashed lines in inset show location of spreading axis. (b) Lineation interpretation from Hydrosweep data. Red lines show the neovolcanic zone. Magnetic anomaly interpretation is summarized in Figure 2.

the magnetic anomalies flanking this spreading segment are not correlatable.

[16] The seafloor that flanks the spreading center adjacent to the Vityaz megamullion is characterized by complex morphology and uncorrelatable magnetic anomalies (Figure 6). The abyssal hill fabric southwest of the axial valley is disturbed by a series of shallow basins located along the northwest edge of the megamullion (Figure 7). Similarly, several V-shaped basins that point south toward the eastern Vityaz fracture zone are located northeast of the ridge. Both zones of disturbed fabric originate at a 12-km axial discontinuity at 5.15°S. The discordant off-axis fabric thus likely represents the fossil trace of this second-order, nontransform discontinuity, similar to discordant zones that originate at second-order discontinuities in the Atlantic [*Grindlay et al.*, 1991; *Sempere et al.*, 1993]. On the basis of the length of its fossil trace, the 5.15°S axial discontinuity has persisted for at least the past 3 Ma.

[17] In contrast to the axial valley at the northeast end of the Vityaz transform fault, the spreading segment at the southwest end of the transform (Figure 8) is characterized by a relatively shallow axial valley (see inset to Figure 8), well defined abyssal hill fabric, and strongly lineated, correlatable magnetic anomalies. These characteristics are interpreted along other spreading centers as evidence for sustained higher melt production and hence magma-dominated seafloor spreading [*Macdonald et al.*, 1991; *Sempere et al.*, 1993]. Numerous small seamounts, most arranged along axis-parallel volcanic ridges, populate the axial valley, in strong contrast to the relatively disorganized arrangements of seamounts within the axial valleys at the northeastern end of the Vityaz transform fault and both ends of the Vema transform fault. The abundance of seamounts indicates that seamount volcanism plays an important role in the accretionary process in this spreading segment, as also appears to be the case along parts of the Mid-Atlantic ridge [*Smith and Cann*, 1992].

## 3.3. Vema Transform Fault and Vicinity

### 3.3.1. Transform Valley

[18] The Vema transform fault offsets the ridge by 240 km, representing a 15 Ma age offset [*DeMets et al.*, 2005]. Reaching a maximum depth of more than 6400 m, the southwestmost 120 km of the transform valley has average depths of 6000 ± 300 m (inset to Figure 9). Depths then shallow

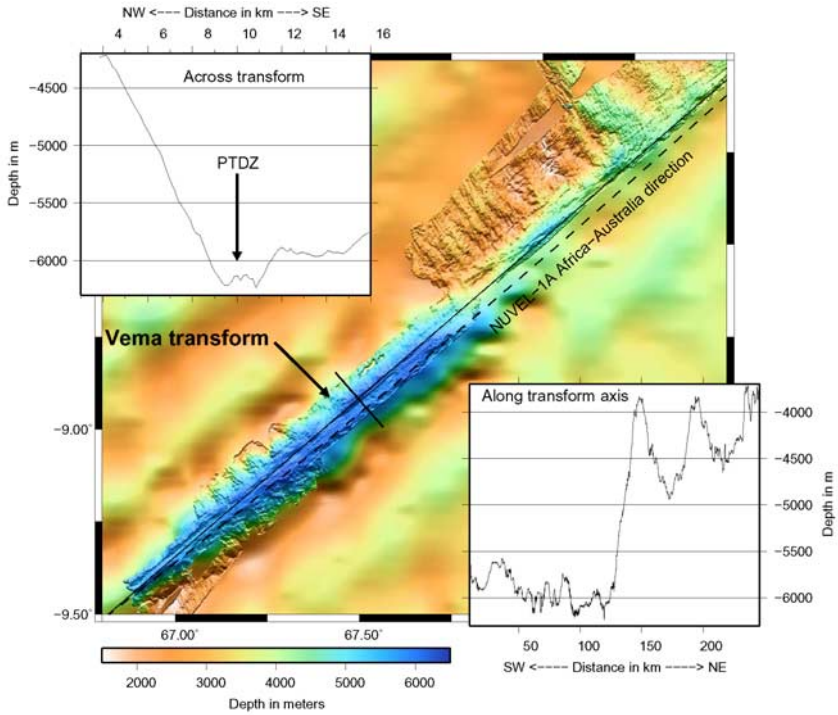


**Figure 9.** Hydrosweep seafloor bathymetry and depth profiles along and across the Vema transform fault. Black lines indicate locations of the along-axis and cross-fault depth profiles shown in the insets.

abruptly to 4250 ± 500 m (inset to Figure 9) along the northeastmost 120 km of the valley for reasons that are unclear.

[19] Our incomplete multibeam coverage of the transform valley precludes any determination of the location of the PTDZ along the entire length of this long transform. Multiple closely spaced lineations in the transform valley can however be traced continuously for ~160 km (Figures 9 and 10) and are likely the present focus of strike-slip motion (the PTDZ). Because these lineations are imaged by multibeam tracks that run both parallel and orthogonal to the transform fault, they cannot be artifacts caused for example by a faulty sonar beam. A small circle around the NUVEL-1A Africa-Australia pole (Figures 9 and 10) parallels the apparent PTDZ, with differences in their traces of no more than a few hundred meters over a distance of more than 100 km. The lineations thus appear to record Africa-Australia slip.

[20] Due to the extreme depth of the transform valley, features on the transform valley floor are best visualized using low-angle, illuminated perspective views (Figures 10–12). A view toward the northeast of the deepest areas of the transform valley (Figure 10) shows snub-nosed abyssal hills truncated against the valley walls and isolated features rising up to 500 m above the valley floor. The topography on the floor of the Vema transform valley is almost certainly caused by some combination of intra-transform volcanism and serpentinite diapirism due to volumetric expansion of hydrating mantle beneath the transform valley, as is the case for Pacific and Atlantic basin transform faults whose valley floors and walls have been observed and sampled directly [e.g., *OTTER Scientific Team*, 1985].

[21] The network of recent fault traces that link the two ridge-transform intersections consists of a 1-km-wide, linear zone of disrupted features along the axis of the Vema transform valley (Figure 10). The fresh-looking geomorphologic character of several well-defined lineations (labeled L1–L4 in Figures 11 and 12) in this 1-km-wide zone, including their slope steepness and continuity, indicate that they likely accommodate present-day slip. A fifth lineation (L5) that is located ~1 km southeast of lineations L1–L4 has a more subtle and less continuous geomorphic expression but can nonetheless be traced as a semicontinuous feature for more than 50 km; we interpret this lineation (L5) as an abandoned PTDZ.

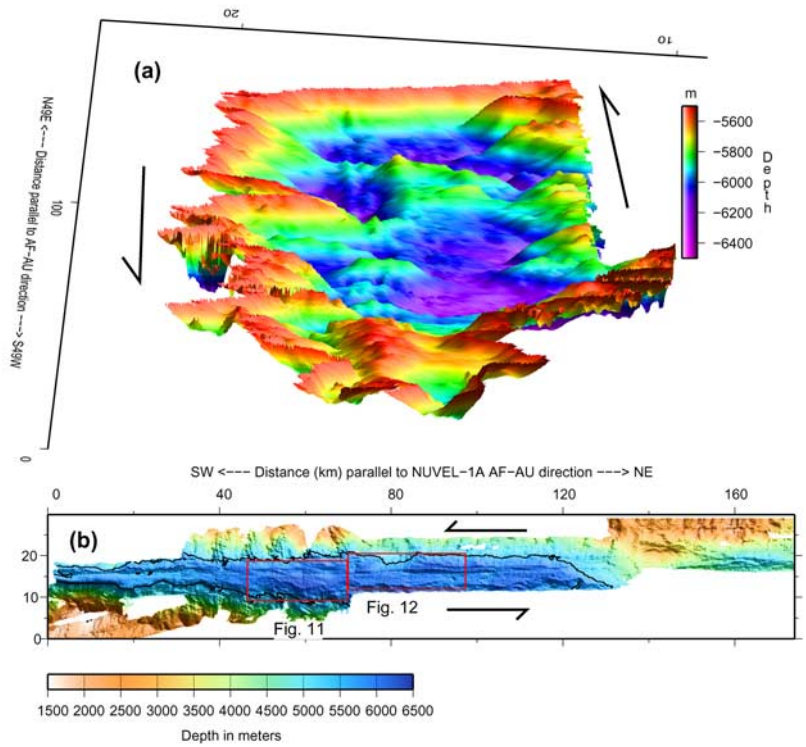


**Figure 10.** (a) Northeast-looking perspective view of areas of the Vema transform valley deeper than 5500 m. (b) Oblique Mercator view of the Vema transform valley projected around the NUVEL-1A Africa-Australia pole. Map location is shown in Figure 3. Horizontal lines are lines of pure slip. Areas outlined in red are displayed in Figures 11 and 12.

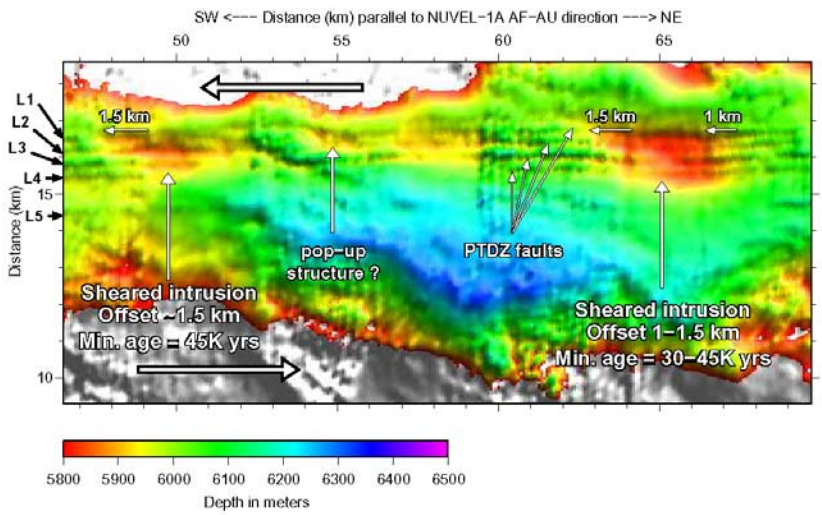


**Figure 11.** Close-up view and interpretation of Vema transform bathymetry. Data are extracted from the oblique Mercator grid shown in Figure 10 and cover the rectangular area from X = 46 km to 70 km and Y = 9–18.5 km. The principal transform displacement zone (PTDZ) consists of four closely spaced, continuous faults (L1–L4) that are actively shearing either serpentinite or volcanic intrusions on the valley floor. Lineation L5 is interpreted as an abandoned PTDZ. Areas where features are better resolved represent areas where orthogonal overlapping multibeam swaths were collected.

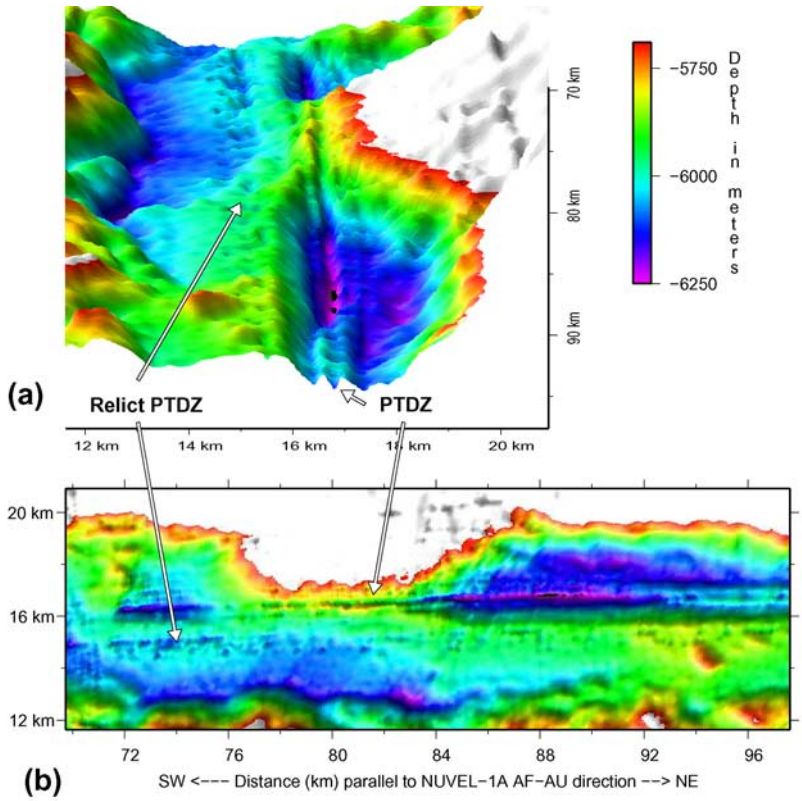


**Figure 12.** (a) Perspective view of Vema transform valley. Data are from the rectangular area from X = 71 km to 97 km and Y = 12–20.5 km extracted from the oblique Mercator grid shown in Figure 10. (b) Map view of area depicted in Figure 12a. The active and relict PTDZs are the continuations of lineations L1–L4 and lineation L5 from Figure 11.

[22] Lineations L1–L4 appear to offset in a left-lateral sense two serpentinite or volcanic intrusions that they cross-cut (located at X = 48–52 km and X = 63–67 km in Figure 11), consistent with the known sinistral sense of slip along the Vema transform fault. Given the small along-fault dimensions of these presumed intrusions (~4 km) and the rapid rate at which they are offset by the PTDZ (33 ± 1 km $Myr^{-1}$), they would be sheared into elongated structures relatively quickly if they were not young. A crude estimate of the offsets needed to restore these two features to roughly elliptical or rectangular shapes is 1–1.5 km (Figure 11), thereby implying that lineations L1–L4 have not been offsetting them for more than 30,000–45,000 years.

[23] Lineations L1–L4 also cut through the lower end of an abyssal hill that extends into the transform valley (Figure 12). The fresh-looking morphologies of the fault trace where it cuts this abyssal hill and of the narrow, steep-sided basins that mark the trace of the PTDZ on both sides of the abyssal hill (perspective view in Figure 12) contrast markedly with the more subtle geomorphic expression of lineation L5. If lineation L5 was abandoned as the PTDZ in the past few tens of thousands of years, marking the possible onset of motion along lineations L1–L4, then its already-muted geomorphic appearance implies rapid modification via mass wasting and possibly intrusive processes. By implication, the Vema transform valley floor and its tectonized zone are dynamic environments in which features are modified over geologically brief intervals. Direct submersible observations of transform valleys in the Atlantic and Pacific ocean basins [*Karson and Dick*, 1983; *Fox and Gallo*, 1984; *OTTER Scientific Team*, 1985] clearly establish that serpentinite intrusion, volcanism, and mass wasting modify features in the transform valley on millennial or shorter time scales, thereby implying a

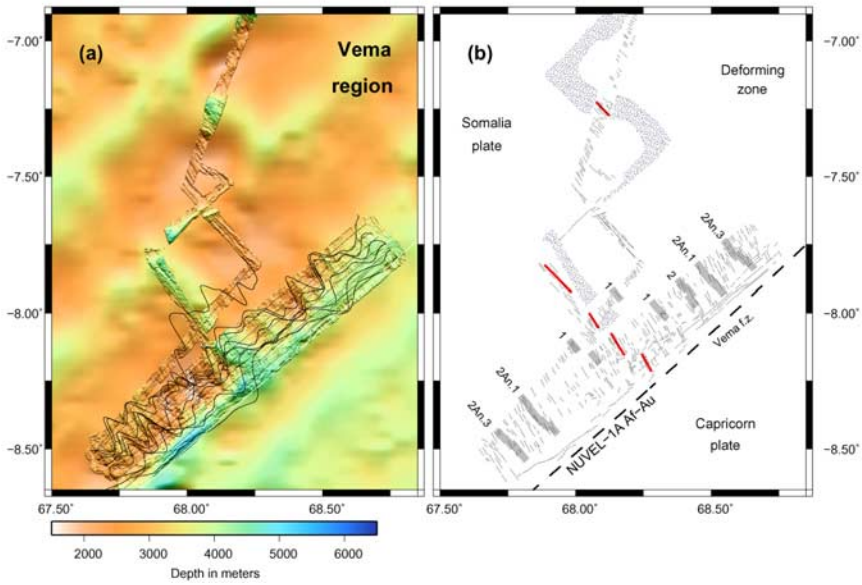


**Figure 13.** (a) Hydrosweep seafloor bathymetry and magnetic anomalies for spreading segments at northeast end of the Vema transform fault. Positive magnetic anomalies point to the northwest. (b) Lineation interpretation. Red lines show the neovolcanic zone. Magnetic anomaly interpretation is summarized in Figure 2.

rapid demise for geological features that are not tectonically active.

### 3.3.2. Spreading Segments

[24] Figure 13 shows multibeam coverage and lineation interpretations for the seafloor spreading segment at the northeast end of the Vema transform fault. The northeastern RTI is morphologically similar to the spreading segment that intersects the northeastern end of the Vityaz transform fault (Figure 6), with a steep-walled axial valley that reaches depths of more than 4000 m and a rugged, inner corner high. Despite their morphological similarity, the magnetic anomalies created along this segment are easily correlated (Figure 2), presumably due to dominantly magmatic extension and a continuous, uninterrupted axial valley.

[25] Hydrosweep coverage of the 35-km-long spreading segment at the southwest end of the Vema transform fault (Figure 14) indicates that the axial valley is narrower and shallower at the middle of the segment than at either of its ends, similar to the spreading segments at either end of the Sealark transform fault. The Hydrosweep data also cover ~25 km of the active part of Fracture Zone O (Figure 14), where well-defined lineaments likely define the PTDZ. Coarser-resolution bathymetry based on satellite altimetry suggests that the transform fault associated with Fracture Zone O has a left-stepping extensional jog near 10.05°S, 66.05°E (Figure 14).

## 4. Kinematic Analysis

[26] We next employ seafloor spreading magnetic anomalies, transform fault orientations, and abyssal hill orientations to quantify the kinematics of deformation within the diffuse Somalia-India-Capricorn triple junction. The analysis is done in two stages. We first use the abyssal hill fabric and transform lineations to quantify variations in seafloor spreading directions as a function of location and time, determine the magnitude of spreading obliquity, and test whether seafloor within the deforming zone east of the spreading axis shows any evidence for pervasive shear or other deformation with respect to undeformed abyssal hill fabric on the Somalia plate west of the spreading axis. We then use the transform lineations and seafloor spreading rates to study the transition from India-Somalia to Capricorn-Somalia motion across the diffuse triple junction.

### 4.1. Fabric Analysis

[27] Abyssal hills record the ridge-normal component of the plate slip direction at the time they are created and thus provide a relatively instantaneous snapshot of plate opening directions everywhere

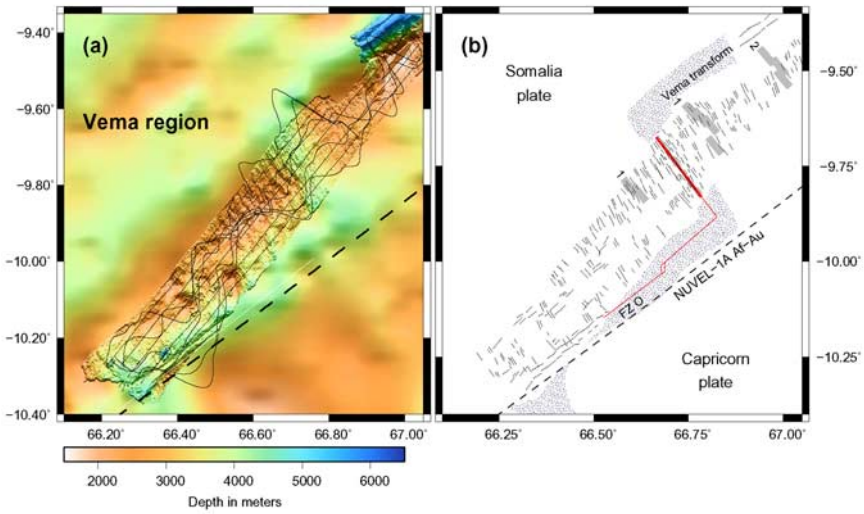


**Figure 14.** (a) Hydrosweep seafloor bathymetry and magnetic anomalies for spreading segments at southwest end of the Vema transform fault. Positive magnetic anomalies point to the northwest. (b) Lineation interpretation. Thick red line indicates the neovolcanic zone. The existence of a left-stepping extensional jog is inferred from coarser-resolution bathymetry based on satellite altimetric measurements. Thin red line shows plate boundary location interpreted from coarse bathymetry.

along a ridge. In contrast, fracture zone ''fabrics'' average plate slip directions over a period equal to the fracture zone age offset, which is frequently several million years or longer. Abyssal hill lineations thus provide a more detailed and potentially more accurate record of changes in plate opening directions. For example, *Cande et al.* [1995] use abyssal hill orientations to map in detail temporal changes in Pacific-Antarctic opening directions, and further demonstrate that the abyssal hill orientations are consistent with the predictions of a detailed model for Pacific-Antarctic seafloor spreading.

[28] Figure 15 summarizes lineations we interpreted from the multibeam data. Overall, we identified 2814 lineations, 95% of which have lengths that range from 0.5 km to 4 km. The individual lineation azimuths for the four subregions into which we divided the data exhibit one-sigma scatters of 10–15° (Figure 15). The azimuths of shorter lineations, which are sensitive to errors in identifying and digitizing their end-points, exhibit significantly more scatter with respect to the mean than do the azimuths of longer lineations.

[29] An important assumption for the analysis below is that individual abyssal hills were parallel to the paleo-spreading axis at the time the abyssal hills were created. The orientations of abyssal hills located within tens of kilometers of a transform fault are however frequently rotated with respect to the orientations of abyssal hills more distant from the transform fault, presumably in response to localized changes in stresses near transform faults [*Phipps Morgan and Parmentier*, 1984; *Sonder and Pockalny*, 1999]. To guard against such a directional bias in our lineation analysis, we divided the abyssal hill lineations into two subgroups based on their distance from the nearest transform fault or fracture zone (Table 1). For the two northernmost regions, the mean orientations for these subgroups agree to within 0.5° (Table 1). Mean directions for the two southernmost subgroups differ by 8.4° and 7.7°, but in opposite senses. There is thus no pattern consistent with a bias in the near-transform abyssal hill orientations. Below, we exclude the orientations of abyssal hills within 15 km of a fracture zone, but note that none of our results would change significantly if we chose instead to include those data.

[30] We assessed the robustness of results derived from the abyssal hill orientations by comparing mean directions that we derived from eight geographically distinct subsets of the data (Table 1), based on the four regions shown in Figure 15 and further subdivided by plate. The mean lineation directions derived from these eight data subsets agree well. For example, the mean directions from

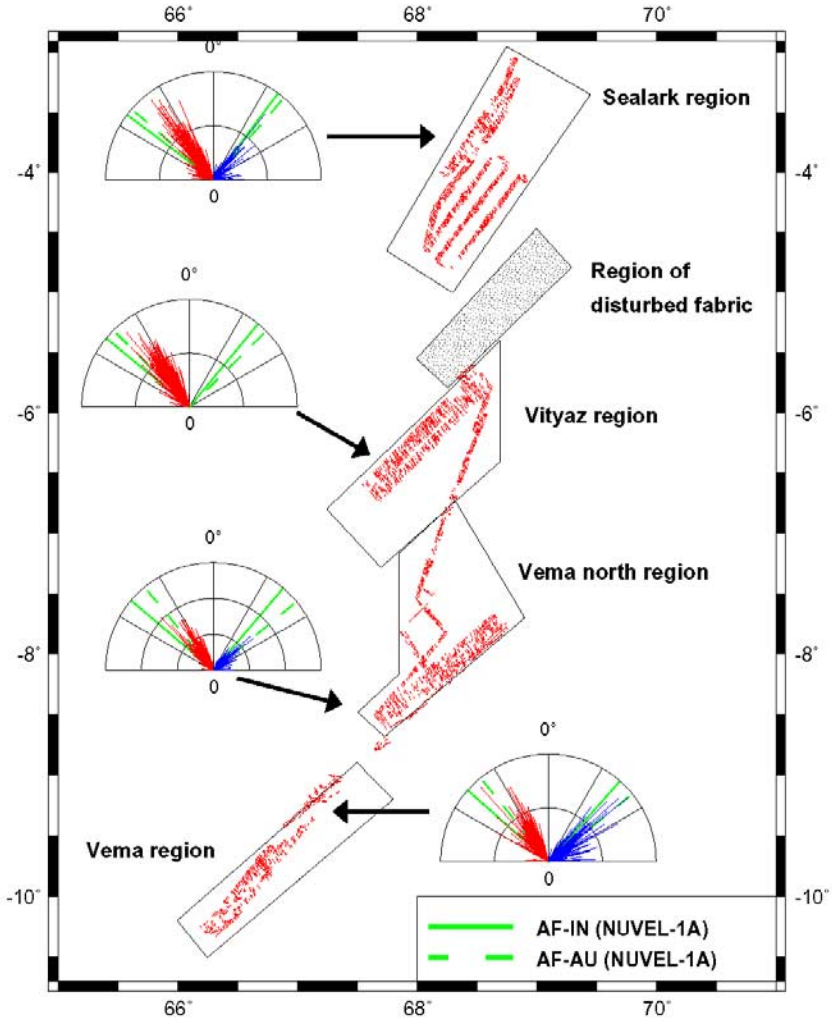


**Figure 15.** Fabric analysis windrose diagrams, which display directions (N90°W–N90°E) and lineation lengths. Lineations for abyssal hills located within 15 km of a transform fault or fracture zone are omitted to avoid introducing any systematic directional bias associated with distributed deformation near the transform fault. Red and blue lines in the windrose diagrams represent abyssal hill and transform fault lineations, respectively.

the Somalia plate and deforming zone east of the ridge agree within 5° for all four regions for lineations farther than 15 km from the fracture zones, and to better than 1° in three out of the four regions if we employ all of the abyssal hill lineations. Within each region, the mean directions derived from lineations on different sides of the spreading center agree to within 1–3°. We interpret the good agreement as evidence that our mean lineation azimuths are robust and thus useful for the kinematic analysis.

[31] Three interesting patterns emerge from the lineation azimuths. The mean abyssal hill and transform fault directions (Figure 16) differ consistently by angles of 95–102°, thereby indicating that spreading is 5°–12° oblique everywhere within the survey area. The sense of obliquity reduces the length of the transform faults and increases the length of the spreading segments relative to that expected for purely orthogonal spreading. This agrees with the pattern that is observed along other seafloor spreading centers where oblique spreading occurs [*Atwater and Macdonald*, 1977]. The obliquity presumably minimizes the ratio of energy that is dissipated along the transform fault relative to that along the ridge [*Stein*, 1978]. Due to this obliquity, the abyssal hill fabric cannot be used as a proxy for the true plate slip direction.

**Table 1.** Abyssal Hill Lineation Analysis

| Plate | Mean Lineation Directions[a] | | | |
|---|---|---|---|---|
| | Sealark | Vityaz | Vema (N) | Vema (S) |
| *All Abyssal Hill Lineations* | | | | |
| Deforming zone | −34.9 | −35.6 | −33.7 | −32.6 |
| Somalia | −35.5 | −32.3 | −33.9 | −32.7 |
| *Excludes Lineations Within 15 km of f.z.* | | | | |
| Deforming zone | −34.8 | −35.6 | −38.4 | −25.6 |
| Somalia | −35.2 | −32.3 | −34.3 | −30.6 |
| *Lineations Within 15 km of f.z.* | | | | |
| Deforming zone | −35.2 | −35.8 | −30.0 | −35.3 |
| Somalia | −35.9 | −32.5 | −32.6 | −33.7 |

[a] Directions are given as degrees clockwise from north. Means are determined from the azimuths of individual lineations weighted by their lengths such that longer lineations contribute accordingly more to the means.

[32] The abyssal hills show little or no systematic variation in their orientations as a function of their ages (Figure 17) and within errors, suggest an approximate upper bound of 5° in any post-4 Ma change in the regional opening direction. The apparently constant opening direction over the past 4 Ma agrees with independent kinematic evidence for nearly steady opening rates and directions since 4 Ma across the Carlsberg and Central Indian ridges [*DeMets et al.*, 2005].

[33] Finally, we find no evidence that the orientations of abyssal hills located on the Somalia plate differ systematically from those located in the deforming zone east of the ridge (Table 1, Figure 16). For the four subregions we considered, the mean abyssal hill directions in the deforming zone differ from those on the Somalia plate by only 0.6°, 3.3°, 0.2°, and 0.1°. This implies that deformation associated with distributed India-Capricorn motion east of the spreading axis does not significantly alter the orientations of abyssal hills by either rigid block rotation or pervasive shearing of the crust.

## 4.2. Kinematic Analysis of Transform Fault and Magnetic Anomaly Data

[34] The new multibeam constraints on transform fault orientations from 3°S–10°S and numerous shipboard and airborne crossings of the magnetic lineations in the deforming zone provide a more complete view of present-day plate motions in the deforming zone (Figure 18) than is available from prior studies. With respect to Africa-India and Africa-Australia velocities predicted by NUVEL-1A, the new kinematic data display an unexpected pattern. The transform fault directions are well fit by the Africa-Australia model everywhere within the survey area (Figure 18a), whereas the 2.6 Ma-average opening rates within the deforming region north of the Vema transform fault are instead well fit by the Africa-India model (Figure 18b).

[35] One possible, though unlikely explanation for these apparently conflicting results is that there are significant errors in the NUVEL-1A estimates for one or both of the Africa-India and Africa-Australia angular velocity vectors. This seems unlikely for a number of reasons. Numerous, well-constrained kinematic data and strong closure around the Australia-Africa-Antarctic plate circuit constrain the NUVEL-1A estimate of Africa-Australia opening rates and directions. More recent models for Africa-Australia motion that employ more numerous, higher-quality data [*DeMets et al.*, 1994a] and consider motion during many different time intervals over the past 20 Ma [*DeMets et al.*, 2005] predict the same motion within uncertainties as NUVEL-1A. The NUVEL-1A Africa-India angular velocity vector is constrained by fewer data and weaker circuit closures, but also predicts motion close to that predicted by more recent models. For example, a newly derived model for Africa-India motion that employs more than 8000 crossings of Carlsberg Ridge magnetic anomalies predicts Africa-India motion of 34.3 ± 0.3 mm $yr^{-1}$ toward N41°E at 8°S, in the same direction and only 1 mm $yr^{-1}$ slower than predicted by NUVEL-1A at that location (S. Merkouriev and C. DeMets, Constraints on Indian plate motion since 20 Ma from dense Russian magnetic data: Implications for Indian plate dynamics, submitted to *Geochemistry, Geophysics, Geosystems*, 2005). The newer Africa-India model thus predicts rates that are in even better agreement with the 2.58 Ma-average rates (Figure 18) than are the rates predicted by NUVEL-1A.

[36] The apparently conflicting kinematic observations described above can be reconciled by a model in which lithosphere within the India-Capricorn deforming zone is assumed to rotate about the India-Australia pole at angular rotation rates that increase monotonically from one edge of the deforming zone to the full angular rate at the far edge. Such a model is suggested by the existence of distributed seismicity along the fracture zones east of the ridge (Figure 1). In this model, the velocity **v** at any point within the deforming zone **r**

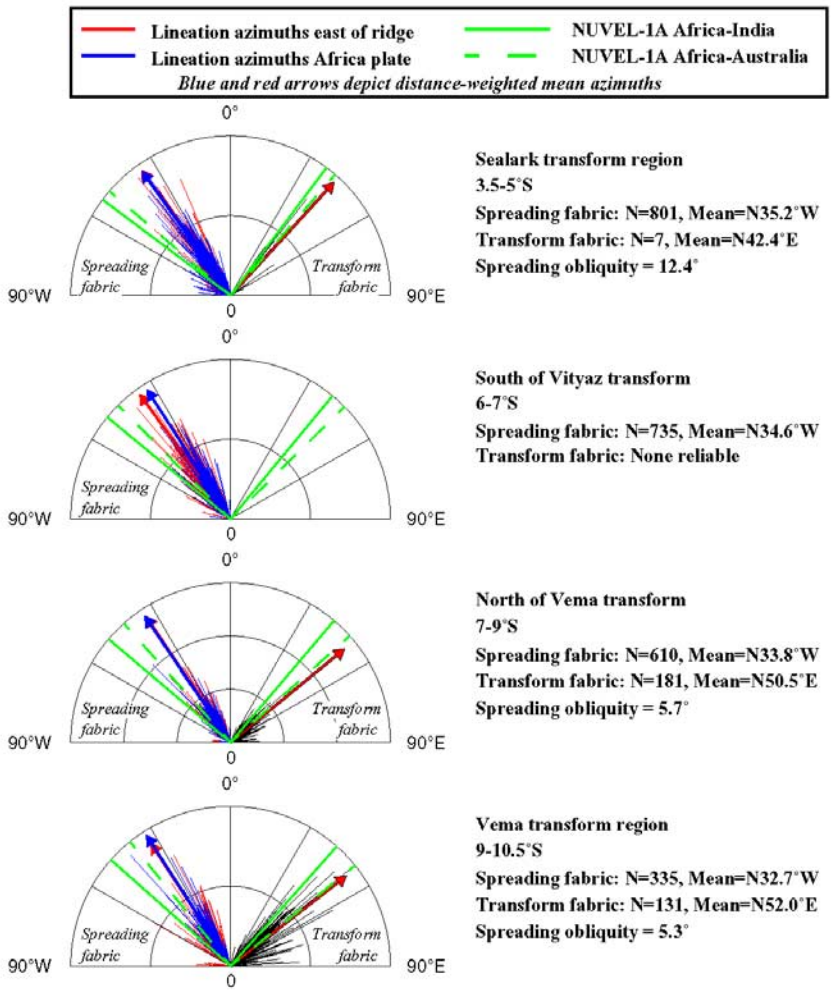


**Figure 16.** Windrose diagrams for fabrics, with separate mean abyssal hill directions for the India and Somalia (Africa) plates (red and blue arrows respectively), mean transform fabric directions (red and black arrows), and predicted plate slip directions. Lineations for abyssal hills located within 15 km of a transform fault or fracture zone are omitted.

is given by $\mathbf{v} = \hat{\Omega}\omega(\mathbf{r}) \times \mathbf{r}$, where $\hat{\Omega}$ is the axis of rotation and $\omega(r)$ is an angular rotation rate that varies with location depending on the nature of the velocity gradient [*Minster and Jordan*, 1987].

[37] Below, we assume that the axis of rotation that describes motion across the deforming zone coincides with the NUVEL-1A India-Australia pole, which is located directly east of the Chagos-Laccadive ridge east of the deforming zone. The NUVEL-1A India-Australia pole location is similar to poles reported more recently by *Gordon et al.* [1990], *DeMets et al* [1994a], *Royer et al.* [1997], and *DeMets et al* [2005]. We approximate the gradient in angular rotation rates by assuming that they increase linearly from one-third of the full rotation rate inside one edge of the deforming zone to the full rotation rate at the far edge.

[38] From the perspective of an observer on the Indian plate (left panel of Figure 19), the above model predicts that lithosphere in the deforming zone moves southward at progressively faster rates ranging from 2 to 5 mm $yr^{-1}$. Summation of the southward-directed linear velocities predicted by this model to velocities predicted by the NUVEL-1A Africa-India angular velocity vector can be used to predict how crust in the deforming zone moves relative to the Somalia plate (Figure 19, second column). Such a model predicts that crust in the deforming zone should move in a direction that is progressively more

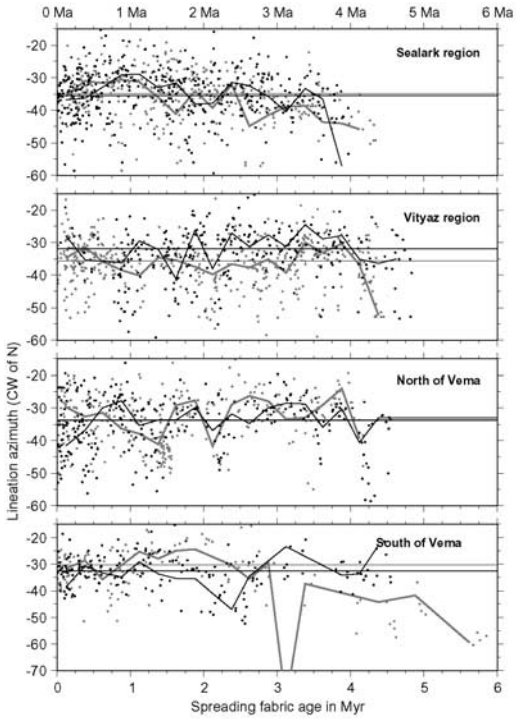


**Figure 17.** Abyssal hill lineation directions (circles) as a function of seafloor age and plate affiliation for the four subregions shown in Figure 15. Horizontal line shows best mean direction for all lineations. Black and gray lines and circles show mean and individual lineation directions for the Somalia plate and seafloor in the deforming zone east of the ridge, respectively. Mean directions are calculated for nonoverlapping 250,000 year age bins.

clockwise from the Africa-India direction for locations that are progressively farther south in the deforming zone. The model also predicts that there should be only a small discrepancy in the opening rate relative to that expected for Africa-India motion. To first order, this correctly predicts the observed pattern of fits and misfits (Figure 18). It fails however to predict the observed clockwise bias in the observed slip directions at the northernmost location (Figure 18).

[39] Relative to an observer on the Capricorn plate (third column in Figure 19), a model in which the rotation rate of lithosphere in the deforming zone increases gradually to the north is also relatively successful at predicting the observed patterns of fits and misfits (Figure 18). Northward increasing motion of the crust in the deforming zone relative to the Australia (Capricorn) plate, when added to Africa-Australia motion, predicts that deforming zone lithosphere will everywhere move in roughly the same direction as the Australian plate relative to Africa (Figure 19), but at rates that are increasingly faster than Australia-Africa rates for locations farther north in the deforming zone. The model once again fails to capture the nature of the misfit at the northernmost deforming location, where the model predicts that lithosphere should move $\sim$2° CCW from the Africa-Australia direction, contrary to the small observed clockwise bias (Figure 18).

## 5. Discussion and Future Work

[40] One clear implication of our analysis is that the present southern limit of the diffuse triple junction coincides with the Vema fracture zone east of the spreading center. The opening rate across the seafloor spreading segment at the southwestern end of the Vema transform fault is fit within errors by the Africa-Australia angular velocity vector, whereas the well-constrained rate for the spreading segment at the northeastern end of the Vema transform fault is poorly fit. Rigid Australian lithosphere thus does not extend north of the Vema fracture zone. Our data do not define the northern edge of the deforming zone, most likely because the multibeam data do not extend far enough north to sample seafloor fabrics that are part of the Indian plate. The deforming zone extends north to at least Fracture Zone H, which ruptured during the $M_s$ = 7.6 July 15, 2003 earthquake and a series of aftershocks.

[41] The unusual pattern of fits and misfits observed for kinematic data from 3°–10°S, in which seafloor spreading rates agree well with motion predicted for the Africa-India plate pair, but transform fault directions agree with motion predicted for the Africa-Australia plate pair (Figure 18), cannot be reconciled with a model in which India-Capricorn deformation over the past several million years has been focused predominantly along one or several closely spaced structures within the deforming zone. The observations are however relatively well explained if we assume that lithosphere within the zone of distributed India-Capricorn deformation obeys a polar deformation field that is centered on the India-Australia rotation pole and is characterized by angular rotation rates that increase gradually across their diffusely deforming boundary. The failure of our simple model to explain the direction of motion of lithosphere near the northern edge of the deforming zone probably results from some combination of errors in our observed directions,

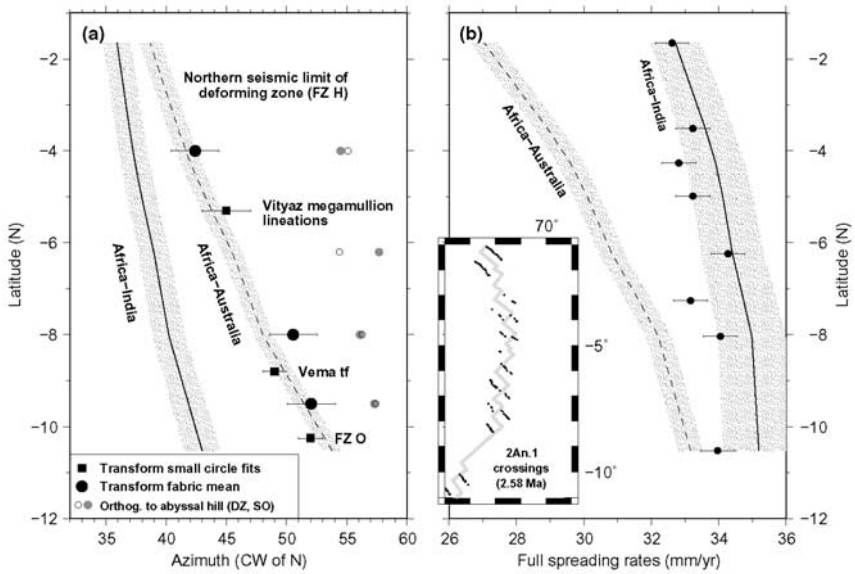


**Figure 18.** Summary diagram of plate kinematic constraints from data analyzed in this study. (a) Plate slip directions with NUVEL-1A Africa-India and Africa-Australia predictions. Mean abyssal hill directions from Somalia plate (gray circles) and seafloor in the deforming zone east of the ridge (small black circles) are from Table 1. Transform slip directions are determined from transform parallel lineations (large solid circles) and best small-circle fits (squares) to the PTDZs for the Vema and other transform faults. The consistent 5°–12° difference between the mean directions orthogonal to the abyssal hills and the mean transform fault fabric directions is a measure of the spreading obliquity. DZ and SO are deforming zone and Somalia plate, respectively. (b) Seafloor spreading rates and NUVEL-1A model predictions for the study area. Individual spreading rates average opening over the width of Chron 2An.1 (2.58 Ma) and are determined from the individual opening angles that best reconstruct crossings of the young edge of anomaly 2An.1 from eight spreading segments shown in the inset. 145 anomaly crossings were employed to estimate the best opening rates. All uncertainties are standard errors.

departures from the assumed polar deformation field and velocity gradient, and possibly errors in the NUVEL-1A India-Australia pole.

[42] Although lithosphere between the southern edge of the Indian plate (possibly coinciding with FZ H) and the presumably discrete northern boundary of the Capricorn plate (coinciding with the eastern Vema fracture zone) clearly moves relative to both the Indian and Capricorn plates, this motion is accommodated in a distributed manner via relative motion between six or possibly more elongated crustal blocks separated by the fracture zones within the deforming zone (Figure 19). In this respect, this diffuse triple junction is unlike other oceanic triple junctions where a microplate separates the major bounding plates (e.g., the Galapagos and Juan de Fernandez triple junctions). To first order, the patterns of deformation and seafloor fabrics associated with the Galapagos [*Lonsdale*, 1988] and Juan de Fernandez [*Larson et al.*, 1992] microplates result from interactions between these internally rigid microplates and their major bounding plates. No comparable internally rigid microplate exists east of the Central Indian ridge.

[43] Our results suggest several obvious avenues for future work in this region. Additional well constrained transform fault directions are needed to establish the northern limit of the India-Capricorn deforming zone, better determine the nature of the deformation gradient, and derive better constrained estimates of present-day Africa-India and hence India-Capricorn motion. Of the ten transform faults that are located between the equator and the Vema transform fault at 9°S, our results are based on partial surveys of only the Vema and Sealark transform faults and transit crossings of two other faults. Surveys of all ten faults and their fracture zones, ideally extending to ages of more than 20 Ma on either side of the ridge, are needed. Ocean bottom seismometers or moored hydrophones deployed in the deforming zone might also provide useful information about off-axis microseismicity that could reveal the locations and distribution of active faults. Finally, mapping of the fracture zones and abyssal hills

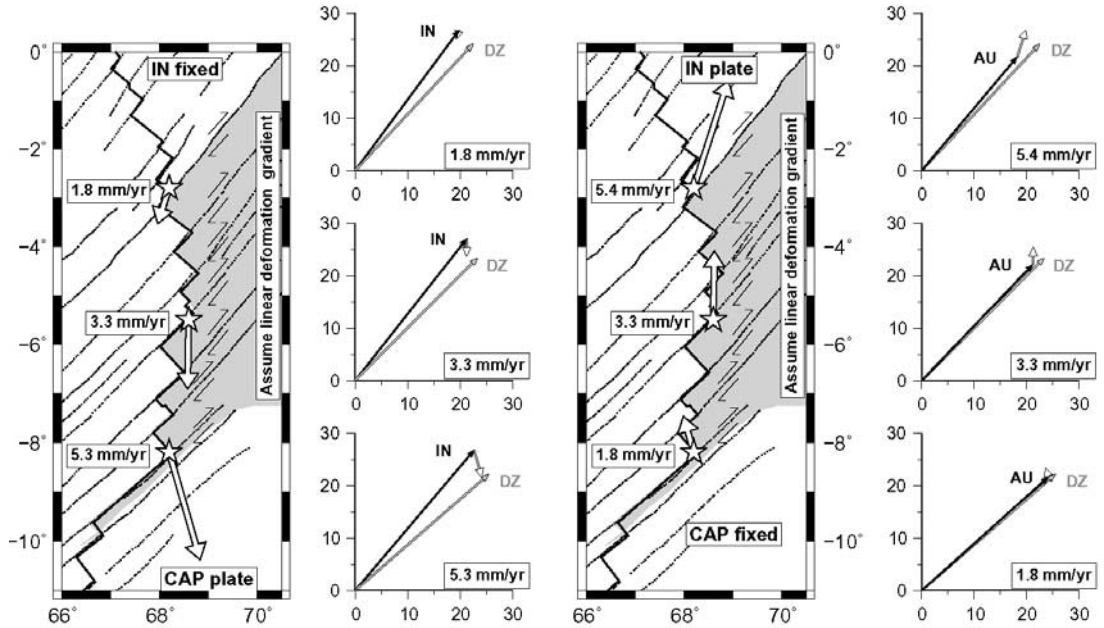


**Figure 19.** Interpretive and linear velocity diagrams for distributed deformation in the triple junction region. Maps show velocity gradients (bold open arrows) determined from an assumed polar deformation model for fixed Indian (leftmost map) and fixed Capricorn plates (rightmost map) using a pole of rotation coincident with the NUVEL-1A India-Australia pole. For the India-fixed model (left), the rotation rate of lithosphere in the deforming zone is assumed to increase progressively from one-third of the full India-Australia angular rate at the northernmost point to the full angular rate at the southern edge of the deforming zone. For the Capricorn-fixed model (right), the motion of lithosphere in the deforming zone is assumed to increase in a similar fashion from the southern to the northern edge of the deforming zone. Linear velocity diagrams to the right of their respective maps compare Indian (IN) and Australian (AU) plate motions predicted by NUVEL-1A relative to the African plate at the three designated points (stars) to observed velocities (shaded) of deforming zone lithosphere (DZ) taken from Figure 18.

older than 4 Ma on both sides of the spreading axis, preferably to ages as old as 20 Ma, would provide additional information about the evolution through time of the distributed deformation.

## 6. Conclusions

[44] The new Hydrosweep and marine magnetic data described above provide useful new information about the spreading axis and transform morphology from 3°S–10°S and the kinematics of deformation across the wide India-Capricorn plate boundary where it intersects the northern Central Indian ridge. The general characteristics of seafloor in the survey region, including deep axial valleys, well-defined abyssal hill fabric, and abundant seamounts within the axial valley are similar to those for the Mid-Atlantic ridge, which has comparably slow seafloor spreading rates. A long-lived and apparently active megamullion adjacent to the Vityaz transform fault is the first described for this region and has characteristics typical of megamullions reported elsewhere. Multibeam coverage of the 240-km-offset Vema transform fault reveals a narrow principal transform displacement zone that can be traced continuously for more than ~150 km within the transform valley. Detailed images of the Vema transform valley floor reveal elevated regions likely to be serpentinite or volcanic intrusions, some of which are offset by the PTDZ and may be only several tens of thousands of years old.

[45] Our analysis of abyssal hill orientations indicates that little or no reorientation of the abyssal hills occurs after they move out of the axial valley. Slip along seismically reactivated fracture zones east of the ridge thus does not appear to cause rigid body rotation or pervasive shearing of the intervening abyssal hills. Abyssal hill orientations have remained relatively constant for the period 0–4 Ma, suggesting that the plate opening direction has not changed during this period. The good fit of the NUVEL-1A Africa-India angular velocity vector to

opening rates throughout the deforming zone and good fit of the Africa-Australia angular velocity vector to plate slip directions throughout the survey area cannot be explained by a model where India-Capricorn motion is focused in a narrow zone where it intersects the ridge. The pattern of fits and misfits to the well-constrained plate slip directions and seafloor spreading rates is however well explained by a model in which lithosphere within the deforming region east of the ridge rotates about the NUVEL-1A India-Australia rotation axis at rates that increase monotonically from zero at one edge of the deforming zone to the full angular rate at the far edge.

## Acknowledgments

[46] We thank Magali Billen, Rob Pockalny, and an anonymous reviewer for comments that led to significant improvements of the manuscript. This work was supported by NSF International grant INT-0244894 (C.D.) and an Indian DST grant to R. K. Drolia. Figures were drafted using GMT software [*Wessel and Smith*, 1991].

## References

Atwater, T., and K. C. Macdonald (1977), Are spreading centres perpendicular to their transform faults?, *Nature*, *270*, 715–719.

Bergman, E. A., and S. C. Solomon (1984), Source mechanisms of earthquakes near mid-ocean ridges from body waveform inversion: Implications for the early evolution of oceanic lithosphere, *J. Geophys. Res.*, *89*, 11,415–11,441.

Cande, S. C., C. A. Raymond, J. Stock, and W. F. Haxby (1995), Geophysics of the Pitman fracture zone and Pacific-Antarctic plate motions during the Cenozoic, *Science*, *270*, 947–953.

Caress, D. W., and D. N. Chayes (1996), Improved processing of Hydrosweep DS multibeam data on the R/V *Maurice Ewing*, *Mar. Geophys. Res.*, *18*, 631–650.

DeMets, C., R. G. Gordon, and P. Vogt (1994a), Location of the Africa-Australia-India triple junction and motion between the Australian and Indian plates: Results from an aeromagnetic investigation of the Central Indian and Carlsberg ridges, *Geophys. J. Int.*, *119*, 893–930.

DeMets, C., R. G. Gordon, D. F. Argus, and S. Stein (1994b), Effect of recent revisions to the geomagnetic reversal timescale on estimates of current plate motions, *Geophys. Res. Lett.*, *21*, 2191–2194.

DeMets, C., R. G. Gordon, and J.-Y. Royer (2005), Motion between the Indian, Capricorn, and Somalian plates since 20 Ma: Implications for the timing and magnitude of distributed lithospheric deformation in the equatorial Indian Ocean, *Geophys. J. Int.*, *161*, 445–468.

Dick, H. J. B., G. Thompson, and W. B. Bryan (1981), Low angle faulting and steady-state emplacement of plutonic rocks at ridge-transform intersections, *Eos Trans. AGU*, *62*, 406.

Drolia, R. K., I. Ghose, A. S. Subramanyam, M. M. Malleswara Rao, P. Kessarkar, and K. S. R. Murthy (2000), Magnetic and bathymetric investigations over the Vema Region of the Central Indian Ridge: Tectonic implications, *Mar. Geol.*, *167*, 413–423.

Drolia, R. K., S. D. Iyer, B. Chakraborty, V. N. Kodagali, D. Ray, S. Misra, R. Andrade, K. Sarma, R. P. Rajasekhar, and R. Mukhopadhyay (2003), The northern Central Indian ridge: Geology and tectonics of fracture zone-dominated spreading ridge segments, *Current Sci.*, *85*, 290–298.

Fox, P. J., and D. G. Gallo (1984), A tectonic model for ridge-transform-ridge plate boundaries: Implications for the structure of oceanic lithosphere, *Tectonophysics*, *104*, 205–242.

Gordon, R. G., C. DeMets, and D. F. Argus (1990), Kinematic constraints on distributed lithospheric deformation in the equatorial Indian Ocean from present motion between the Australian and Indian plates, *Tectonics*, *9*, 409–422.

Grindlay, N. R., P. J. Fox, and K. C. Macdonald (1991), Second-order ridge axis discontinuities in the south Atlantic: Morphology, structure, and evolution, *Mar. Geophys. Res.*, *13*, 21–50.

Kamesh Raju, K. A., T. Ramprasad, and C. Subrahmanyam (1997), Geophysical investigations over a segment of the Central Indian Ridge, Indian Ocean, *Geo Mar. Lett.*, *17*, 195–201.

Karson, J. A., and H. J. B. Dick (1983), Tectonics of ridge-transform intersections at the Kane Fracture Zone, *Mar. Geophys. Res.*, *6*, 51–98.

Kuo, B. Y., and D. W. Forsyth (1988), Gravity anomalies of the ridge-transform system in the South Atlantic between 31° and 34.5°S: Upwelling centers and variations in crustal thickness, *Mar. Geophys. Res.*, *10*, 205–232.

Larson, R. L., R. C. Searle, M. C. Kleinrock, H. Schouten, R. T. Bird, D. F. Naar, R. I. Rusby, E. E. Hooft, and H. Lasthiotakis (1992), Roller-bearing tectonic evolution of the Juan Fernandez microplate, *Nature*, *356*, 571–576.

Lin, J., G. M. Purdy, H. Schouten, J. C. Sempere, and C. Zervas (1990), Evidence from gravity data for focused magmatic accretion along the Mid-Atlantic Ridge, *Nature*, *344*, 627–632.

Lonsdale, P. (1988), Structural pattern of the Galapagos microplate and evolution of the Galapagos triple junctions, *J. Geophys. Res.*, *93*, 13,551–13,574.

Macdonald, K. C., D. S. Scheirer, and S. M. Carbotte (1991), Mid-ocean ridges: Discontinuities, segments and giant cracks, *Science*, *253*, 986–994.

Minster, J. B., and T. H. Jordan (1987), Vector constraints on western U.S. deformation from space geodesy, neotectonics, and plate motions, *J. Geophys. Res.*, *92*, 4798–4804.

OTTER Scientific Name (1985), The geology of the Oceanographer transform fault: The transform domain, *Mar. Geophys. Res.*, *7*, 329–358.

Phipps Morgan, J., and E. M. Parmentier (1984), Lithospheric stress near a ridge-transform intersection, *Geophys. Res. Lett.*, *11*, 113–116.

Pockalny, R. A., R. S. Detrick, and P. J. Fox (1988), The morphology and tectonics of the Kane transform from Sea Beam bathymetry data, *J. Geophys. Res.*, *94*, 3179–3194.

Ranero, C. R., and T. J. Reston (1999), Detachment faulting at ocean core complexes, *Geology*, *27*, 983–986.

Royer, J.-Y., R. G. Gordon, C. DeMets, and P. R. Vogt (1997), New limits on the motion between India and Australia since chron 5 (11 Ma) and implications for lithospheric deformation in the equatorial Indian Ocean, *Geophys. J. Int.*, *129*, 41–74.

Sandwell, D. T., and W. H. F. Smith (1997), Marine gravity anomaly from Geosat and ERS 1 satellite altimetry, *J. Geophys. Res.*, *102*, 10,039–10,054.

Schouten, H., and K. McCamy (1972), Filtering marine magnetic anomalies, *J. Geophys. Res.*, *77*, 7089–7099.

Sempere, J.-C., J. Lin, H. S. Brown, H. Schouten, and G. M. Purdy (1993), Segmentation and morphotectonic variations along a slow spreading center: The Mid-Atlantic ridge (24°00′N–30°40′N), *Mar. Geophys. Res.*, *15*, 153–200.

Shaw, W. J., and J. Lin (1996), Models of ocean ridge lithospheric deformation: Dependence on crustal thickness, spreading rate, and segmentation, *J. Geophys. Res.*, *101*, 17,977–17,993.

Smith, D. K., and J. R. Cann (1992), The role of seamount volcanism in crustal construction at the Mid-Atlantic ridge (24°–30°N), *J. Geophys. Res.*, *97*, 1645–1658.

Sonder, L. J., and R. A. Pockalny (1999), Anomalously rotated abyssal hills along active transforms: Distributed deformation of oceanic lithosphere, *Geology*, *27*, 1003–1006.

Stein, S. (1978), A model for the relation between spreading rate and oblique spreading, *Earth Planet. Sci. Lett.*, *39*, 313–318.

Tchalenko, J. S. (1970), Similarities between shear zones of different magnitudes, *Geol. Soc. Am. Bull.*, *81*, 1625–1640.

Tucholke, B. E., J. Lin, and M. C. Kleinrock (1998), Megamullions and mullion structure defining oceanic metamorphic core complexes on the Mid-Atlantic Ridge, *J. Geophys. Res.*, *103*, 9857–9866.

Wessel, P., and W. H. F. Smith (1991), Free software helps map and display data, *Eos Trans. AGU*, *72*, 441–446.

White, R. S., R. S. Detrick, M. C. Sinha, and M. H. Cormier (1984), Anomalous seismic crustal structure of oceanic fracture zones, *Geophys. J. R. Astron. Soc.*, *79*, 779–798.

Wiens, D. A. (1986), Historical seismicity near Chagos: A complex deformation zone in the equatorial Indian Ocean, *Earth Planet. Sci. Lett.*, *76*, 350–360.

Wiens, D. A., and S. Stein (1984), Intraplate seismicity and stresses in young oceanic lithosphere, *J. Geophys. Res.*, *89*, 11,442–11,464.

Wiens, D. A., et al. (1985), A diffuse plate boundary model for Indian Ocean tectonics, *Geophys. Res. Lett.*, *12*, 429–432.